

Aqueous-phase reforming of water-soluble compounds from pyrolysis bio-oils

Jéssica Justicia, José Alberto Baeza, Adriana S. de Oliveira, Luisa Calvo, Francisco Heras*, Miguel A. Gilarranz

Chemical Engineering Department. Universidad Autónoma de Madrid. Ciudad Universitaria de Cantoblanco, 28049, Madrid, Spain

ARTICLE INFO

Keywords:

Aqueous-phase reforming
Bio-oil
Aqueous fraction
Water soluble
Hydrogen
Pt/C catalyst

ABSTRACT

Aqueous-phase reforming (APR) of model compounds of bio-oil aqueous fraction (AFB) was studied at different operating conditions. Substrate conversion, carbon-to-gas yield (CCgas) and hydrogen and alkanes production were evaluated. Levoglucosan, hydroxyacetone, furfural and acetic acid were selected as representative of AFB and tested in batch APR at different concentrations (1–5 %wt.), temperatures (175–220 °C) and reaction times (0.5–4 h), using 3% (wt.) Pt/CB catalysts. Best results were obtained at 220 °C and 1%, with 70–90% substrate conversions, 45–70% CC gas and hydrogen production up to 50 mmol per gram of total organic carbon (TOC). Catalyst stability was checked in APR of levoglucosan during five successive 4 h reaction cycles. The catalyst exhibited high stability, CCgas remained constant and hydrogen production increased and became stable after first reaction cycle with only a slight decrease of TOC conversion. The catalyst with well dispersed metal phase and high contribution of nanoparticles smaller than 2 nm showed a higher production of hydrogen. APR was proved to be a feasible option for the valorisation of AFB.

1. Introduction

With the focus in a decarbonized future, research in waste biomass valorisation has received increasing attention [1]. One of the most promising valorisation methods is pyrolysis [2], which produces three product streams: gas (mainly composed by CO, CO₂, CH₄ and H₂), bio-oil and biochar. Several works have been focused on the production of gas, due to its good properties for use as biofuel, and biochar, which can be used as fuel, adsorbent, soil amendment, etc. [3–5]. The recovery and use of bio-oil is more challenging because it is composed of an organic and an aqueous fraction, both containing a complex mixture of compounds [6].

The organic fraction of bio-oil contains mainly phenolic compounds and lignin derivatives, including hydroxymetilfurane, phenol and phenolic compounds (guaiacol, cresol, etc.), organic acids (hexadecenoic, octadecanoic) and methyl esters of these acids, among others [1,7,8]. The composition of bio-oil aqueous fraction (AFB) is highly variable, depending mainly on the starting biomass and the pyrolysis conditions. However, most works in literature reported a reduced number of components as the most frequent, namely levoglucosan, acetic acid, furfural and hydroxyacetone (acetol). Table 1 shows

proximate quantitative composition of AFBs obtained from different types of biomass. The water content in all cases is as high as 80–90%, and none of the four main components appears in a concentration higher than 5% (wt.), although their concentration can change substantially depending on the initial biomass used. Remon et al. [9] studied the aqueous phase of the bio-oil produced by fast pyrolysis of pine wood in fluidized bed and spouted bed reactors, observing similar composition in both cases, with levoglucosan and hydroxyacetone as the components at higher concentration. In the case of the work by Black et al. [10] on fast pyrolysis of oak wood the main components of AFBs were levoglucosan and acetic acid.

The composition and high water content of AFB poses important challenges for the valorisation and recovery of the chemicals contained in this fraction. Thus, the use of AFB as biofuel would require costly removal of water. In this context, aqueous-phase reforming (APR) can be considered a promising method for the valorisation of AFB. As in the case of steam reforming (SR), APR consists essentially in the reaction between an organic substrate and water to produce hydrogen and carbon monoxide, but in APR the reaction takes place in the liquid phase [13]. In terms of energy, APR of AFB can be more efficient than steam reforming (SR) because milder operating conditions are used

* Corresponding author.

E-mail address: fran.heras@uam.es (F. Heras).

<https://doi.org/10.1016/j.renene.2022.09.021>

Received 9 May 2022; Received in revised form 5 September 2022; Accepted 6 September 2022

Available online 16 September 2022

0960-1481/© 2022 The Authors. Published by Elsevier Ltd. This is an open access article under the CC BY-NC-ND license (<http://creativecommons.org/licenses/by-nc-nd/4.0/>).

Table 1
Characterization of aqueous fraction of bio-oil obtained for different biomass.

BIOMASS	Composition (% wt.)				
	OAK WOOD		PINE SAWDUST		
Hydroxyacetone	0.3	0.1	1.4	0.7	1.5
Levogluconan	1.1	4.5	3.1	2.0	1.6
Acetic acid	0.6	3.1	3.1	0.7	0.7
Furfural	<0.2	0.2	<0.9	0.1	<0.1
Water	89.9	80.6	82.0	84.0	84.0
Ref.	[11]	[10]	[12]	[9]	[9]

(200–250 °C and 15–30 bar) and evaporation of the feed is not needed [14,15]. At APR conditions the water gas shift reaction (WGS) equilibrium is almost completely displaced to products, yielding a gas product mainly composed by hydrogen and carbon dioxide [16–18]. In addition to reforming and WGS reactions, additional reactions occurring at APR conditions leading to the production of different water-soluble hydrocarbons via Fischer-Tropsch route, hydrogenation and dehydration [19, 20]. APR process can be considered to involve two main routes, namely i) C-C, C-H and O-H bonds cleavage and WGS; and ii) C-O bonds rupture and alkane and formation of carbohydrates such as acids, sugar alcohols, etc. [19,21,22].

Regarding catalysts for APR, the most studied have been Group VIII to X metals due to higher activity in C-C bond cleavage [23–25]. The best results in terms of catalytic activity and selectivity to hydrogen have been found using supported Ni and Pt, with Pt showing much higher stability [18,21,26]. The support also plays an essential role in APR process. In general, acidic and neutral supports promote secondary reactions leading to alkane formation, while basic supports favor WGS and other reactions that increase hydrogen yield [27]. γ -Al₂O₃ has been one of the most widely studied supports for Pt catalysts showing high hydrogen selectivity, although hydration of this material to boehmite at APR conditions leads to an increase in selectivity to alkanes and eventually results in loss of activity [28–30]. Carbon materials have also been shown as interesting supports for APR catalysts because of their tunable textural and chemical structure and thermal stability [30–32].

The most studied APR substrates have been sugar alcohols, including sorbitol, xylitol and glucose, and alcohols, such as glycerol, methanol and ethanol, among others [16,17,33,34]. A higher suitability for hydrogen production has been attributed to substrates with a C:O atomic ratio close to 1 [20].

In the last years, the APR of bio-derived compounds, especially from biorefinery schemes, has received increasing attention. Some works have studied the APR of individual compounds commonly present in bio-oil and AFB. Hydroxyacetone has been one of the most studied model compounds. Some works showed carbon yield to gases of up to 50% in the APR of hydroxyacetone using Ni-Co/Al-Mg catalysts and H₂ content in produced gas higher than 30% [35]. However, hydroxyacetone can also undergo aldol condensation reactions leading eventually to catalyst deactivation by coke formation in Pt/AlO(OH) and Pt/ZrO₂ catalysts [36]. Substantially different results were reported in other works where only 1–2% carbon to gas yield was observed using Ni catalysts supported on alumina, ceria and lanthana [37]. Diverse results have also been reported for the APR of acetic acid, which is among the most refractory compounds in AFB. Nozawa et al. [38] compared the APR of ethanol and acetic acid using Ru/TiO₂ catalysts, achieving four times higher values of TOF for hydrogen production in the case of ethanol. Similar trends were shown by Arandia et al. [39] for the APR of acetic acid and ethanol catalysed by spinel NiAl₂O₄, Ni/CeO₂- γ -Al₂O₃ and Ni/La₂O₃- α -Al₂O₃. Some studied have reported that catalyst deactivation in the APR of acetic acid and ethanol is not relevant [39]. However, Lozano et al. [35], found low reactivity of acetic acid in APR using Ni-Co/Al-Mg catalysts, especially compared to ethanol, due to catalyst deactivation.

As reported in literature, one the main obstacles for the use of APR a

hydrogen source is the cost of the organic compounds used as process feedstock. On the other hand, the high water-content and wide composition in organic matter of AFB makes difficult to develop routes for its valorisation or recovery of components, therefore it is usually considered as a wastewater stream. The current work proposes overcoming both obstacles through the valorisation of AFB by APR to produce biomass-derived hydrogen and alkanes. Processability of different components of AFB is study to determine most favorable compositions for APR process. Likewise, catalyst stability is evaluated since deactivation is a common bottleneck in the valorisation of complex biomasses by APR.

Despite the works commented above, few studies can be found in literature comparing the behavior in APR of main compounds occurring in biorefinery waste streams feeds. The objective of the current work is to explore the APR of bio-oil aqueous fraction with carbon-supported Pt catalysts expanding the number of model compounds considered to assess the role in the processability of AFB. The stability of the catalysts was also evaluated upon five successive applications.

2. Experimental section

2.1. Materials

The chemicals used as bio-oil aqueous fraction model compounds were furfural (98%), levogluconan (98%), hydroxyacetone (95%) and acetic acid (99%) supplied by Merck, Carbosynth Limited, Alfa-Aesar-Thermofisher and Sigma Aldrich, respectively. Hexachloroplatinic acid solution (8 % wt. in water) purchased from Sigma Aldrich was used as precursor salt for catalysts preparation, while carbon black ENSACO 250G supplied by Timcal Canada Inc. (Canada) was used as catalyst support.

On the other hand, ENSACO 250G support is characterized by a relatively ordered structure, which contributes to hydrothermal stability. Likewise, the absence of oxygen in the APR medium minimizes carbon support degradation [40].

2.2. Synthesis and characterization of catalyst

3% (wt.) Pt/CB catalyst was prepared by incipient wetness impregnation. The support was impregnated with the chloroplatinic acid aqueous solution, dried overnight at 60 °C, calcined in air at 200 °C for 2 h and, finally, reduced under H₂ flow at 300 °C for 2 h. This catalyst was selected due to the high activity shown in previous works on the APR of biomass pollutants in wastewater [41]. A 3% (wt) nominal metal load was considered as suitable for assessing the suitability of AFB as a substrate for APR according to the results achieved in previous works on the APR of a variety of substrates [41,60,64].

Fresh catalyst was characterized by N₂ adsorption/desorption at 77 K (Tristar II, Micromeritics). TPD/TPO analyses were performed with TA Instruments SDT 650. TPD were carried out under 50 mL/min N₂ flow, from room temperature to 900 °C using a ramp of 10 °C/min; next, the samples were cooled up to 100 °C and by last, the gas was switched to air without flowrate variation to accomplish the TPO up to the same final temperature using a 5 °C/min ramp. Fresh and used catalysts reduced for 2h were characterized by STEM with a Tecnai F30 microscope (FEI company). Those that were reduced for 3h, with a FEI Talos F200X microscope. Software 'ImageJ 1.51k' was used for counting and measuring Pt nanoparticles on digital STEM images. XPS profiles were recorded using a PHI VersaProbe II instrument equipped with X-ray source, 1486.6 eV at 25.1 W, with a beam diameter of 100.0 μ m. Software 'XPS peak v4.1' was used for the deconvolution of the spectra to obtain the relative amounts of Ptⁿ⁺ and Pt⁰ species. The data analysis procedure involved smoothing, a Shirley background subtraction and mixed Gaussian-Lorentzian by a least-square method for curve fitting. C 1s peak (284.6 eV) was used as internal standard for binding energies corrections due to sample charging.

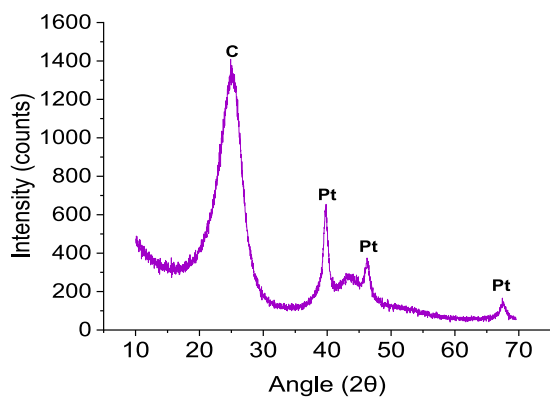


Fig. 1. XRD spectrum of Pt/CB catalyst.

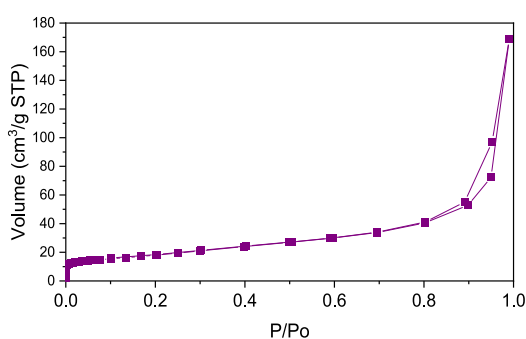


Fig. 2. N₂ adsorption/desorption isotherm at 77 K for fresh catalyst.

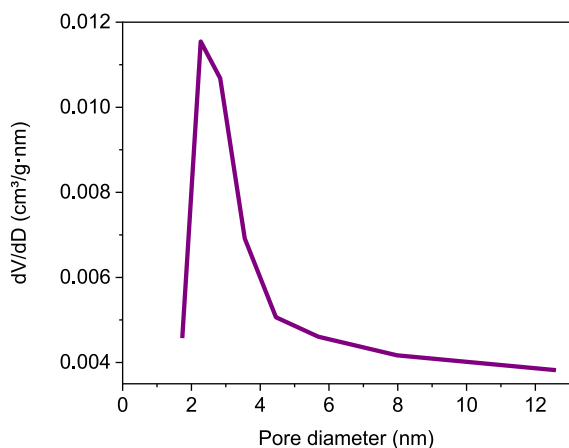


Fig. 3. Pore size distribution (BJH Desorption) for fresh catalyst.

XRD pattern (Fig. 1) was obtained by a Bruker D8 Discover device using monochromic CuK α radiation, an angular range of 20–70°, a step size of 0.02° and a dwell time of 1 s per increment. The broad peak at 25.0° corresponds to (002) band of carbon black support, showing that is predominantly an amorphous carbon, although the peak around 44° is usually ascribed to (200) band and is indicative of small regions with graphitic properties [42]. The sharp peaks at 39.9, 46.5° and 67.6° can be attributed to platinum reflections (111), (200) and (220), respectively, which are consistent with a face centred cubic structure, showing

Table 2

Characterization of support and catalyst used in APR experiments.

Catalyst	S _{BET} (m ² /g)	A _{ext} (m ² /g)	Micropore volume (cm ³ /g)	Mesopore volume (cm ³ /g)	pH slurry
Pt/CB	65	65	<0.001	0.09	8.7
CB	65	65	<0.001	0.09	8.9

the formation of crystalline Pt phase [13,43].

The N₂ adsorption/desorption isotherm and pore size distribution determined from the isotherm by BJH method are shown for the catalyst in Figs. 2 and 3, respectively. The isotherm obtained corresponds to type IV-a according to IUPAC classification, showing very low contribution of microporosity. The BET specific surface area (S_{BET}), external area (A_{ext}) and pore volume of the fresh catalyst and the support are summarized in Table 2. The textural properties of the catalyst are the same to those of the carbon black support, i.e., low specific surface area and microporosity, but noticeable mesoporosity (0.09 cm³/g). A relatively wide pore size distribution was obtained in the narrow mesopore range, extending well beyond 12 nm, with a substantial contribution between 2 and 4 nm. The small particle size (22 μ m) and negligible microporosity of the catalysts and the use of a slurry reactor provided with mechanical stirring contribute to diminished mass transfer constraints.

2.3. APR experiments

The reaction experiments were carried out in a 50 mL Teflon-lined stainless steel reactor vessel that was inserted in a heating block. The reactor was loaded with 15 mL of initial solution and 0.15 g of catalyst. Then, it was sealed and purged three times with Ar. Initial pressure at room temperature was set at 5 bar and magnetic stirring at 750 rpm. The reactor was heated to reaction temperature using a 3 °C/min ramp. After completion of the reaction time, the reactor was cooled down to room temperature. The gas produced was collected in multilayer foil sample bags (Supelco, USA) and analysed in a GC/FID/TCD apparatus (7820 A, Agilent) using two packed columns and a molecular sieve column. The liquid phase produced was characterized by measuring total organic carbon (TOC) with a TOC-VCSH apparatus (Shimadzu).

Previous works on the APR of other substrates using the same catalyst Pt/C indicated good reproducibility of the results. Thus, in APR of brewery and juice production wastewaters, error values were around 5–10% and 10–20% for X_{TOC} and gas product composition, respectively [60,64].

TOC conversion (X_{TOC}), carbon conversion to gas (CC gas), H₂ yield (Y_{H2}), H₂ selectivity (S_{H2}) and alkanes selectivity (S_{ALKANES}) were calculated as:

$$X_{TOC} (\%) = \frac{TOC_{initial} \left(\frac{mg}{L}\right) - TOC_{final} \left(\frac{mg}{L}\right)}{TOC_{initial} \left(\frac{mg}{L}\right)} \times 100 \quad (1)$$

$$CC_{gas} (\%) = \frac{C_{gas} (g)}{C_{initial} (g)} \times 100 \quad (2)$$

$$Y_{H2} = \frac{H_2_{produced} (mol)}{H_2_{theoretical} (mol)} \times 100 \quad (3)$$

$$S_{H2} (\%) = \frac{H_2_{produced} (mol)}{C_{at\ produced} (mol)} \times \frac{1}{R} \times 100 \quad (4)$$

$$S_{ALKANES} = \frac{Alkanes\ produced (mol)}{C_{gas\ produced} (mol)} \times 100 \quad (5)$$

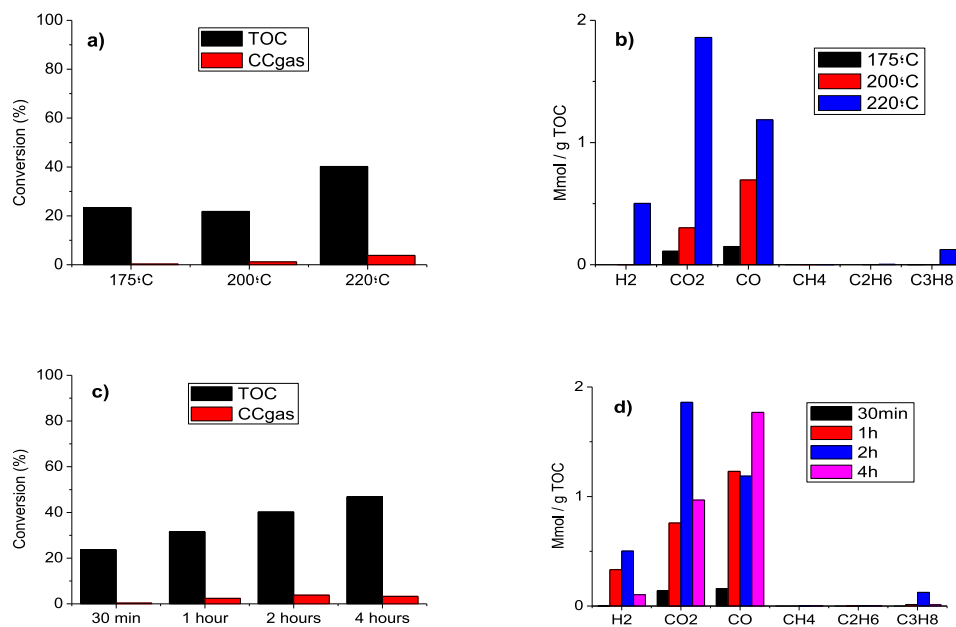


Fig. 4. TOC conversion, CC gas and gas production at: a) and b) different temperature (5% furfural, 2 h) and c) and d) different time (5% furfural, 220 °C).

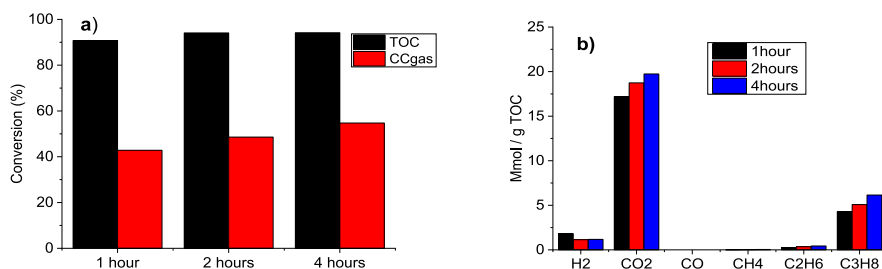


Fig. 5. TOC conversion, CC gas and gas production at different time (1% furfural, 220 °C).

Table 3

Yield and selectivity in the APR of 1% (wt.) furfural at different times (220 °C).

Time (h)	Y_{H_2} (%)	S_{H_2} (%)	$S_{ALKANES}$ (%)
1	1.0	3.4	19.3
2	0.6	1.6	21.5
4	0.7	1.5	23.8

3. Results and discussion

3.1. Selection of operating conditions for APR

Temperature, time and feedstock concentration were studied as the main variables affecting the APR process. Furfural was selected as model compound for assessing their influence. TOC conversion, CC gas and gas composition for the treatment of furfural aqueous solutions at different temperature, time and concentration are shown in Fig. 4 and Fig. 5. Yield and selectivity for 1% (wt.) furfural APR can be observed in Table 3.

In Fig. 4a and b the results of runs at different temperatures are compared. At 175 and 200 °C, CCgas was almost negligible, even though significant TOC conversion could be observed. TOC conversion could be ascribed to the removal of furfural from the liquid phase by

intermolecular aldol condensation and further deposition [44]. Likewise, some removal of furfural by hydrothermal carbonization can be expected from the production of CO and CO₂, particularly at 200 and 220 °C [41,45]. At 220 °C, TOC conversion increased to 49% and CCgas reached around 5% (Fig. 1a). Fig. 4b also show the increase in the production of gases at 220 °C. In all the experiments CO production was higher than the usual values reported for APR, indicating lack of activity of the catalyst in WGS reaction. This could be related to the deposition of condensation products leading to blockage of active sites. An operating temperature of 220 °C was selected for further runs in the view of the gas production achieved.

To assess changes in activity, experiments at different reaction times were carried out. As can be observed in Fig. 4c and d, TOC removal reached ca. 24% after 30 min of reaction, however no significant production of hydrogen and alkanes was detected. Significant CO and CO₂ production was recorded at 30 min, probably indicating early occurrence of reactions leading to condensation and hydrothermal carbonization. Steady conversion of TOC with reaction time was observed. Production of gases also increased, but more significantly in the case of CO and CO₂. It must be noted that Fig. 4 a)-d) show negligible production of methane and ethane, while in former works these gases were produced together with hydrogen in APR of biomass waste compounds [46]. This observation, and the production of CO, suggest constrains for

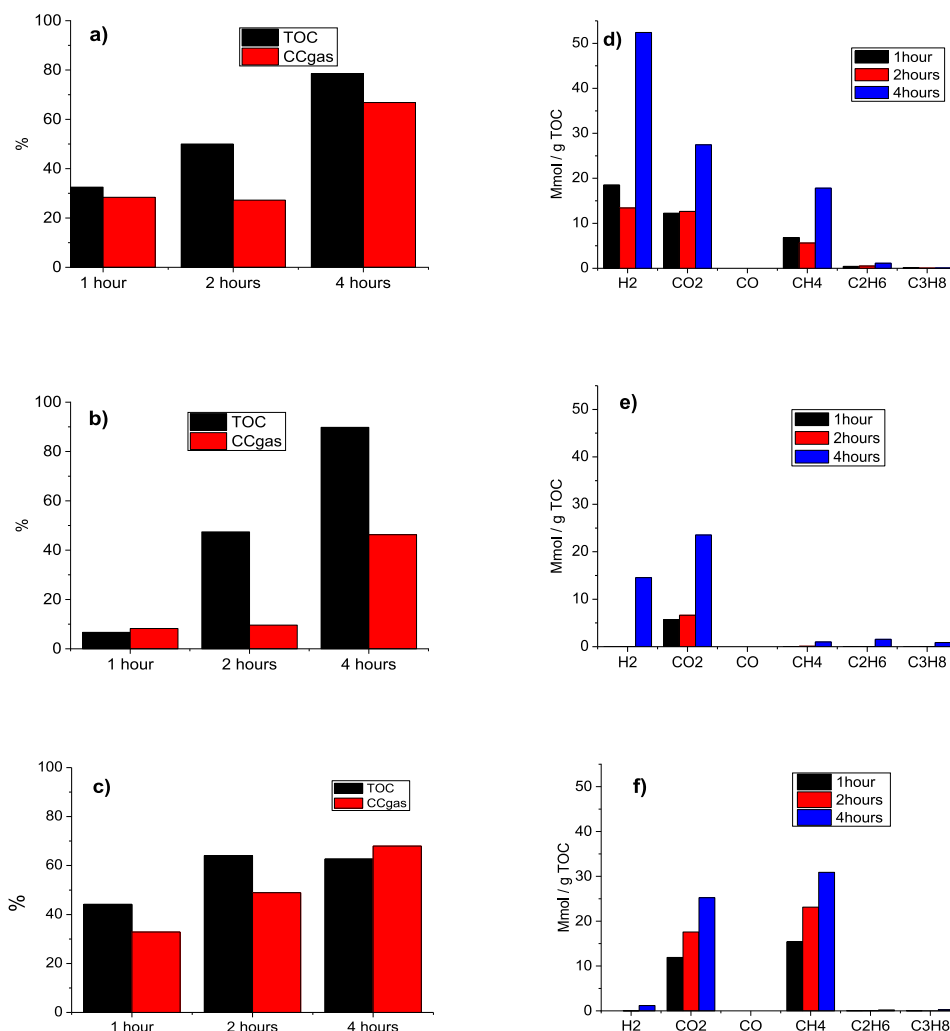


Fig. 6. TOC conversion, CC gas and gas production at different reaction times a) d) Hydroxyacetone, b) e) Levoglucosan, c) f) Acetic acid (1% concentration, 220 °C).

APR reaction, probably due to blockage of active sites at the catalyst. Some authors have previously discussed that polymerization of furfural in an acid medium can result in low hydrogen production [47]. Interestingly, hydrogen is produced despite the lack of activity of the catalyst in WGS reaction. Hydrogen production could be ascribed, at least partially, to a route related to hydrothermal carbon [41].

Condensation reactions leading to blockage of active sites may be promoted by a high concentration of furfural in the reaction medium, therefore additional experiments were carried out with an initial concentration of 1% (wt.). As can be seen in Fig. 5a and b, significantly higher TOC conversion and CC gas values of around 95% and 50%, respectively, were obtained, with a relatively low influence of reaction time. This boost in conversion at low concentration feedstock has also been observed in the APR of other substrates [41,48]. CO₂ and alkanes production were an order of magnitude higher than when 5% (wt.) furfural was used. This observation is in agreement with the studies carried out by Luo et al. [48], who studied the APR of 5 and 10% (wt.) glycerol with Pt- γ -Al₂O₃ and observed better results for 5% solution, in terms of CCgas and hydrogen yield.

The decrease in feed concentration leads negligible presence of CO in gas product stream, showing higher activity of the catalyst in WGS reaction, which also contributes to higher H₂ production. Anyhow, H₂ production and selectivity showed low values for the experiments with

1% (wt.) furfural, about 1 mmol/gTOC and 2%, respectively (Fig. 5 and Table 3). A fraction of the hydrogen produced may be consumed by the furfural side reactions to produce alkanes, in particular propane as shown by gas analysis. Thus, furfural can be hydrogenated in successive reactions to pentane-1,5-diol, with furfuryl alcohol as reaction intermediate [49]. This C5 diol can undergo in turn dehydrogenation/decarbonylation to produce propane [50]. It must be noted that H₂ production was lower than that of alkanes, which is unusual in APR, particularly for Pt catalysts [18,51,52]. Propane production can be considered as an advantage for a hypothetical energy recovery from the gas by combustion.

3.2. APR of individual model compounds

The APR of the main components considered for AFB model composition, i.e. furfural, levoglucosan, acetic acid and hydroxyacetone, was studied using the operating conditions selected from the results of the previous experiments with furfural: 1% (wt.) concentration and 220 °C.

Fig. 6a, b and 6c compare TOC conversion and CCgas at different reaction time. A behaviour similar to that of furfural was observed for hydroxyacetone (Fig. 6a). TOC conversion for this compound increased with reaction time and reached a maximum value c.a. 79% after 4 h,

Table 4

Yield and selectivity in the APR of model compounds (1% concentration, 220 °C).

	Time (h)	Y _{H₂} (%)	S _{H₂} (%)	S' ALKANES (%)
Hydroxyacetone	1	12.3	39.3	19.3
	2	10.2	29.5	19.3
	4	34.9	46.9	18.5
Levogluconan	1	n.d.	n.d.	n.d.
	2	n.d.	n.d.	n.d.
	4	8.5	24.0	8.5
Acetic acid	1	n.d.	n.d.	56.4
	2	n.d.	n.d.	56.7
	4	0.7	1.0	54.2

which is slightly lower than for furfural, however, a CCGas value as high as 67% was obtained at this reaction time. The results of levogluconan APR were strongly dependent on reaction time (Fig. 6b). TOC conversion increased from 6.7 at 1 h to 90% at 4 h. Moreover, CCGas increased from 8% after 1 h to 10% after 2 h, whereas an increase to 46% occurred during the last 2 h of reaction. Finally, relatively high conversion of TOC and CCGas were achieved for acetic acid APR (Fig. 6c), reaching in both cases values close to 65% after 4 h. The CCGas value obtained at 2 h of

reaction (49%) for acetic acid is higher than that reported in other works (33.5% [53]) using a Pt/C catalyst and a similar feed concentration (0.9%), probable due to the higher catalyst/feed ratio used in the current work (10 g catalyst/L vs 5 g catalyst/L). Previous works [54] have also shown that catalyst/acetic acid ratio is an important variable influencing APR of this compound.

Fig. 6d, e and 6f show individual gases production per gram of TOC at different reaction times and Table 4 the yield and selectivity data. Regarding hydroxyacetone, a sharp increase in hydrogen production can be observed with reaction time, from 15 mmol/gTOC at 2 h to more than 50 mmol/gTOC at 4 h. Alkane fraction was mainly composed by methane, whose production reached 20 mmol/gTOC after 4 h of reaction (Fig. 6d). In addition, very high hydrogen selectivity (50%) was obtained at long reaction time (Table 4). The mechanism of hydroxyacetone APR has been previously discussed as part of the overall reaction mechanism of glycerol APR [55]. This mechanism (Fig. 7) would explain the production of hydrogen and methane from hydroxyacetone. Hydroxyacetone can be hydrogenated in several stages to produce methane in the gas phase and undergo hydrogenolysis to generate hydrogen and acetic acid, which in turn can produce more methane [54]. Other authors also reported results of hydroxyacetone reforming,

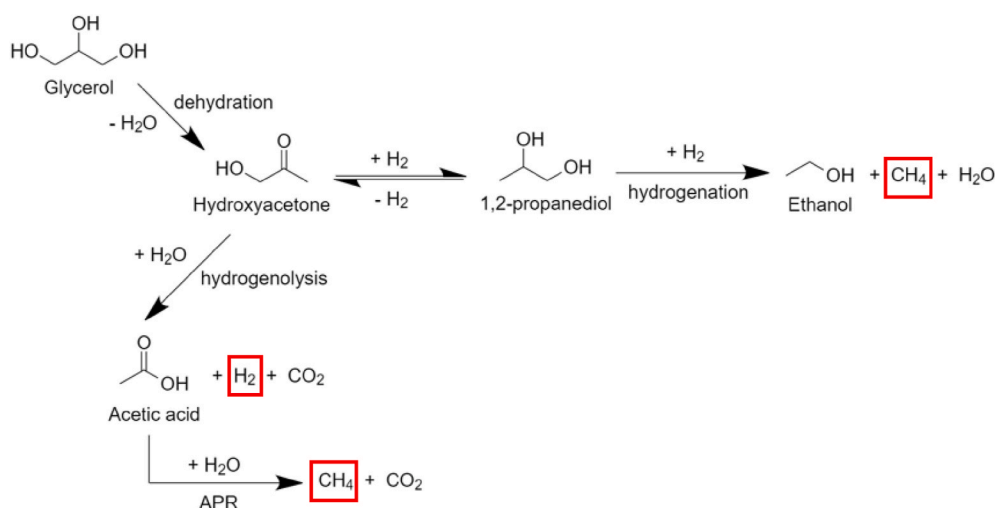


Fig. 7. Mechanism of glycerol APR [50].

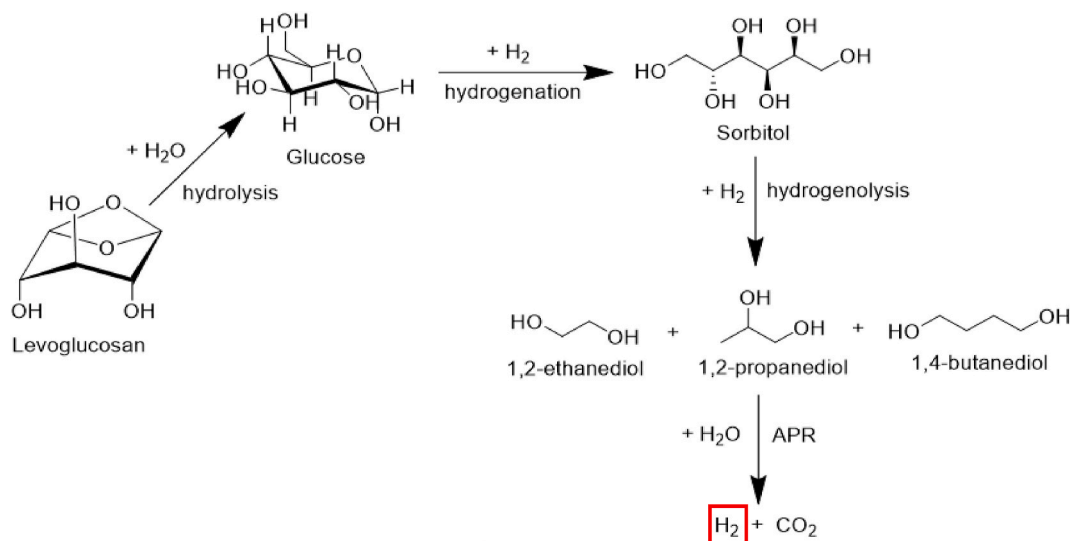


Fig. 8. Transformation of levoglucosan into sorbitol and subsequent hydrogenolysis [57].

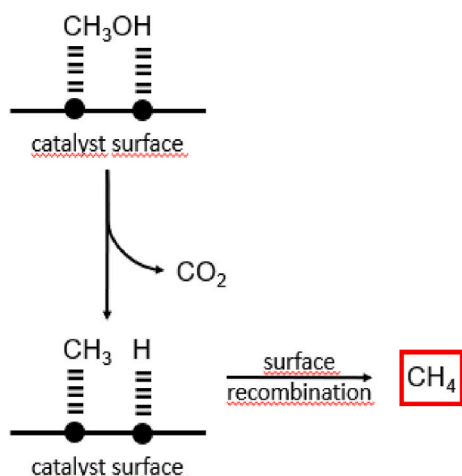


Fig. 9. Proposed reaction mechanism for the APR of acetic acid [49].

showing the presence of both gases, hydrogen and methane [56–58].

Comparing the results obtained in the current work with those reported in literature, Lozano et al. [35] observed CCgas values of 45–50% and hydrogen content in the gas of 33.7% using different catalyst load and similar operating conditions. Callison et al. [55] reported lower hydrogen production values (0.4 mmol H₂ and 0.2 mmol CH₄ vs 5.75 mmol H₂ and 1.96 mmol CH₄), using similar reaction conditions but much higher initial hydroxyacetone concentration (10 vs 1% wt.).

In the case of levoglucosan, the production of alkanes was negligible after 1 and 3 h reaction time, with a slight increase up to 3.4 mmol alkanes/gTOC after 4 h (Fig. 6e). Hydrogen production was only observed to be significant after 4 h, reaching 15 mmol/gTOC. This hydrogen production is higher than that reported by King et al. [59] at 225 °C using Pt/C catalysts (0.4 mol hydrogen/mol levoglucosan vs 1.2 mol hydrogen/mol levoglucosan in the present work), which could be attributed to the type of support used in the current work. Thus, Oliveira et al. [60] observed an important influence of the type of carbon support, and particularly in of pH slurry of the support, in catalysts activity.

The behaviour of levoglucosan could be related to competing hydrolysis reactions taking place during heating of the feed. Thus, it has been shown that under these conditions levoglucosan can be hydrolysed to glucose [11,62]. Helle et al. [61] showed that hydrolysis begins at temperatures as low as 90 °C and can reach high reaction rate. The reaction route can be explained from the chemical pathway proposed for the transformation of glucose to sorbitol by Bindwal et al., showed in Fig. 8 [62]. The hydrolysis to glucose would justify the similarity observed between levoglucosan and glucose APR results. TOC conversion was about 90%, which can be compared with the value of 83% observed by Irmak et al. in the APR of a 4400 ppm glucose solution at

523K with a 5% Pt catalyst [63]. Additionally, gas production and composition were similar to those reported by Saenz de Miera et al. [64] for the APR of 1% glucose at similar operating conditions. Finally, Kaya et al. [65] reported 20% H₂ in the produced gas with glucose as substrate using a 10% Pt/AC catalyst with 13.7 nm metal nanoparticle size. The higher percentage of H₂ obtained in the current work may be due to the smaller metal nanoparticle size ($d_m = 2.2$ nm) in the catalyst.

In the case of acetic acid, there is a slight dependence between TOC conversion and reaction time (Fig. 6c). Hydrogen production was low at all reaction times studied. On the opposite, methane production increased monotonically with time, reaching 30 mmol/gTOC after 4 h (Fig. 6f). Likewise, the selectivity to methane was practically constant over time showing a mean value around 56%. In Fig. 6f it can be observed that the main gaseous product is methane, well above the hydrogen content. Pipitone et al. found an equivalent trend when using platinum-based catalyst in the APR of acetic acid [53,54]. As can be seen in the Fig. 9, acetic acid is transformed into methane by APR through a simple mechanism: first, with a CO₂ removal step, and then through surface recombination [53].

3.3. Catalyst stability and reuse

Fig. 10 shows the results for the reuse of Pt/CB catalyst in five successive 4 h runs at 220 °C, using levoglucosan as model compound. The catalyst was revealed as very stable, since only a moderate decrease of TOC conversion was observed, remaining at 74% of initial value, after the five cycles (Fig. 10a). CCgas remained almost constant at around 40–45%, increasing very slightly with the cycles. In Fig. 10b, it can be observed that the production of hydrogen increased after the first cycle (from 16 to 38 mmol/gTOC), stabilizing at a value of 35 mmol/gTOC after the fifth cycle. In the case of alkanes, generation remained constant in ca. 4 mmol/gTOC. Pipitone et al. [66] also found an improvement in hydrogen selectivity after the second reuse cycle, in the APR of alginate 1% (wt.), using a commercial 3% Pt/C.

For a better understanding of the catalyst performance during the five cycles of reuse, it was characterized by STEM, TGA and XPS. Fig. 11 shows the results of STEM characterization of the Pt/CB catalyst both fresh and used after 1, 3 and 5 cycles.

Well dispersed metal particles can be observed in the images and minor differences were found between fresh and reused catalyst, which allows to rule out relevant sintering influencing Pt catalytic behaviour. However, for the fresh catalyst a narrower nanoparticle size distribution ranging from 0.5 to 4 nm was observed. Some redispersion of the metal phase can be observed after 1 cycle, leading to a higher prevalence of nanoparticles smaller than 2 nm. Within the 5-cycle range studied the catalyst mean nanoparticle size remained around 2 nm but distribution became broader, with a tail extending up to 7.5 nm for the catalysts used in three and five cycles. The increase in the fraction of nanoparticles with larger size can be related to Ostwald ripening, in which growth of

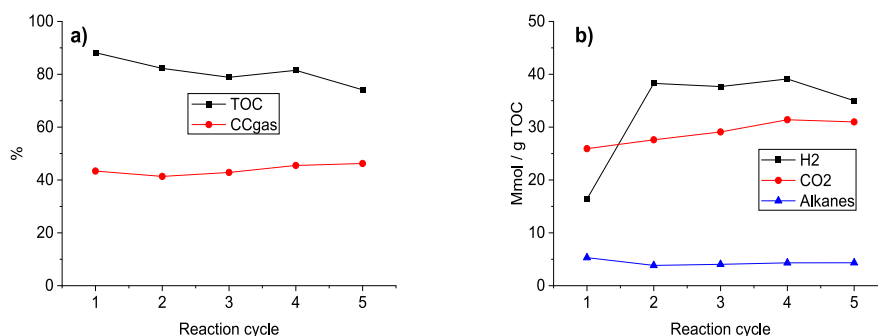


Fig. 10. Pt/CB catalyst stability in five consecutive batch reaction cycles: a) TOC conversion and CCgas, b) Gas production (1% levoglucosan, 220 °C, 4 h).

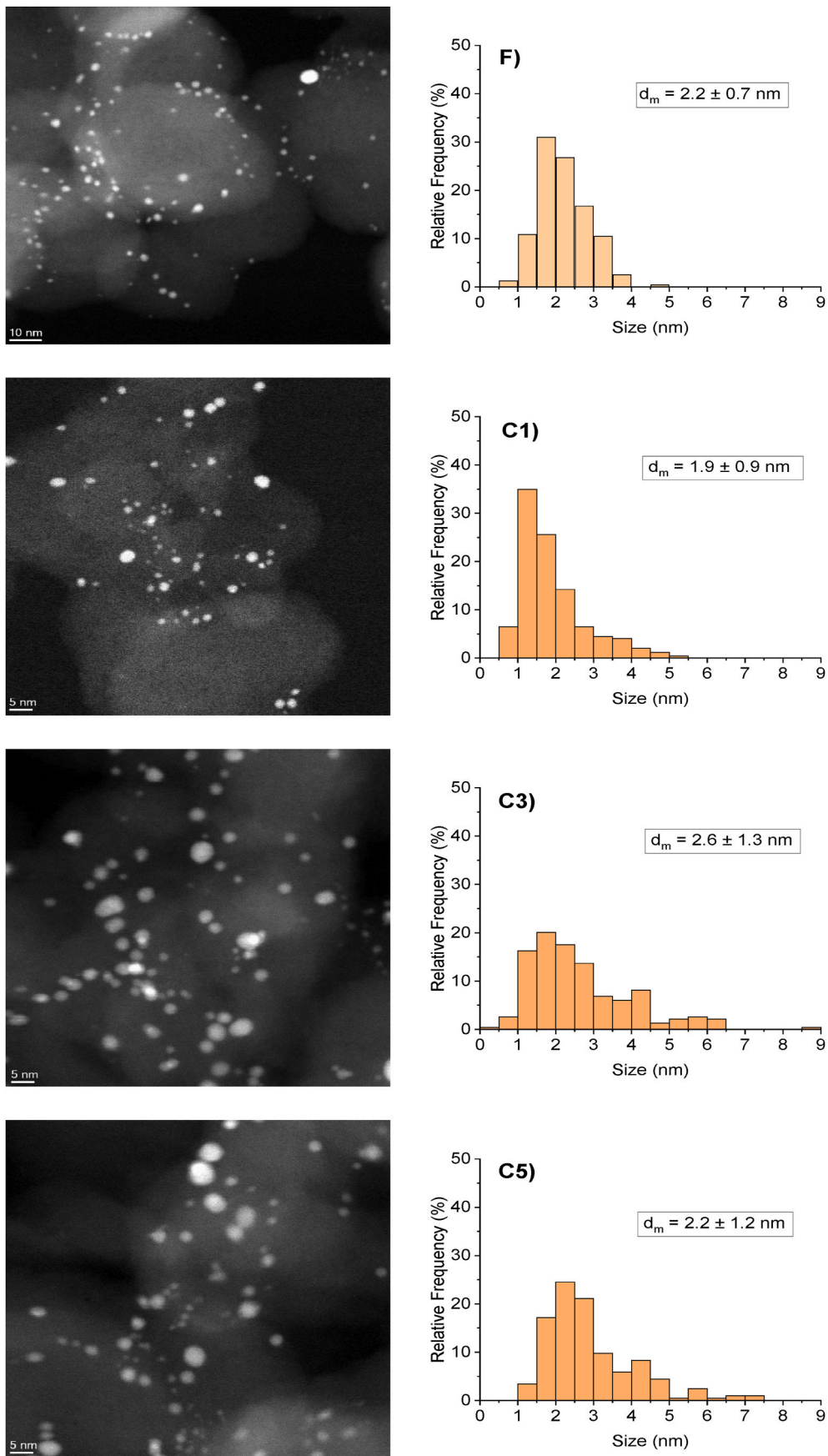


Fig. 11. STEM images of Pt/CB catalyst: F) fresh, C1) cycle 1, C3) cycle 3 and C5) cycle 5.

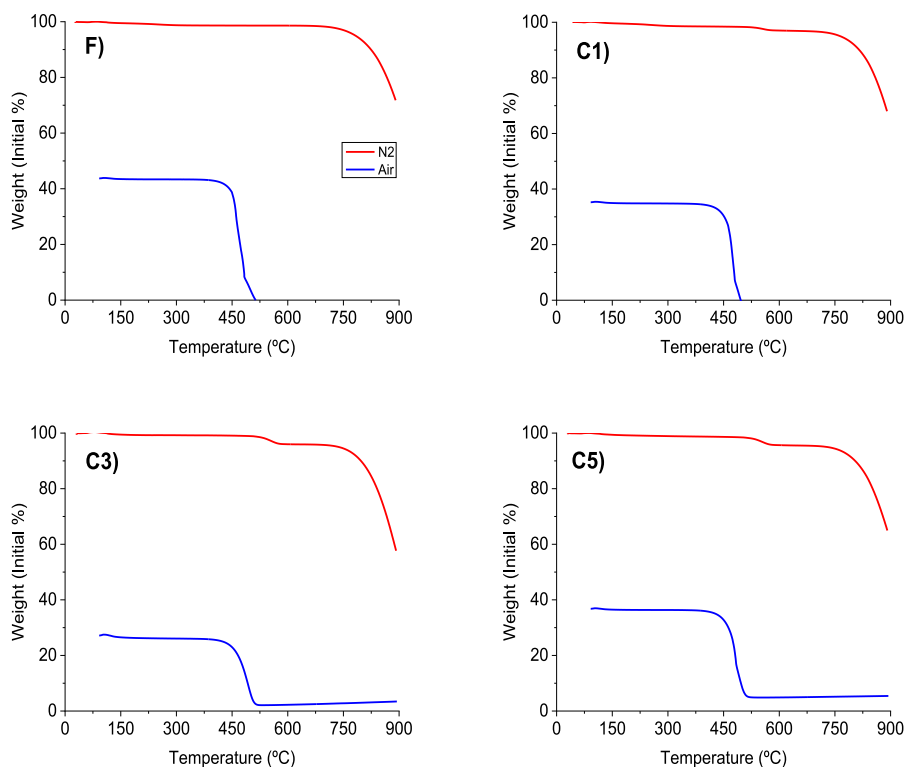


Fig. 12. Thermogravimetric analysis (desorption and oxidation) of Pt/CB catalyst: F) fresh, C1) cycle 1, C3) cycle 3 and C5) cycle 5.

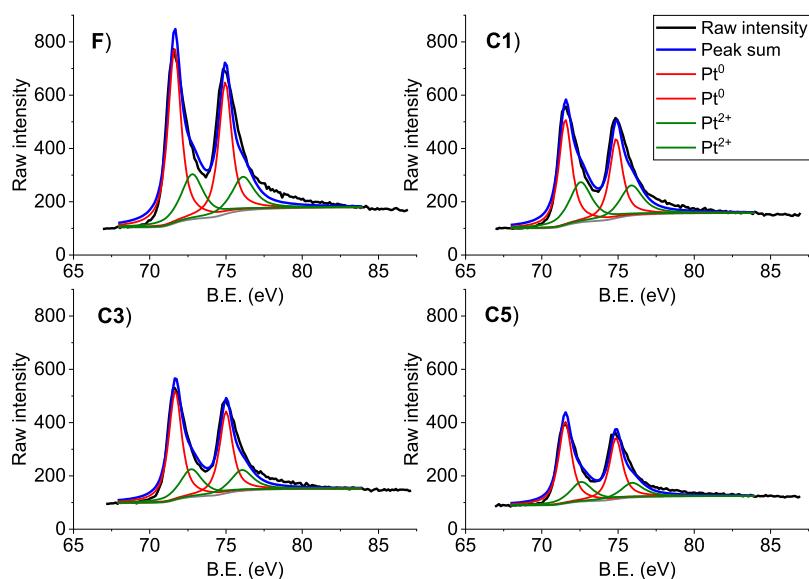


Fig. 13. Platinum (Pt 4f) XPS spectra of Pt/CB catalyst: F) fresh, C1) cycle 1, C3) cycle 3 and C5) cycle 5.

nanoparticles takes place because large particles are more energetically favoured than small ones [67].

As can be seen in Fig. 12, thermogravimetric desorption and oxidation profiles in air were obtained with no remarkable results except a very slight weight loss in inert atmosphere at 500–600 °C, probably due to the deposition of hydrothermal carbon or coke formed during APR on

the catalyst surface. The deposition of coke can contribute to lower activity since TOC conversion was found to decrease [41]. TPO profile for the fresh catalyst show a high stability in air, ascribable to the highly ordered structure of the ENSACO 250G support, with negligible mass loss ascribed to oxidation up to ca. 400 °C. Likewise, TEM images do not indicate degradation of carbon support leading to evident

Table 5

Binding energies (BE) for each species of Pt/C and Pt²⁺/Pt⁰ ratios from Pt 4f XPS spectra for fresh and reused catalyst.

Sample	Species	Binding energy (eV)		Pt ²⁺ /Pt ⁰ ratio
		Pt 4f _{7/2}	Pt 4f _{5/2}	
Fresh catalyst	Pt ⁰	71.62	74.95	0.4
	Pt ²⁺	72.78	76.11	
After cycle 1	Pt ⁰	71.54	74.89	0.7
	Pt ²⁺	72.54	75.87	
After cycle 3	Pt ⁰	71.67	75.00	0.4
	Pt ²⁺	72.71	76.04	
After cycle 5	Pt ⁰	71.53	75.86	0.4
	Pt ²⁺	72.59	75.92	

Table 6

Pt²⁺/Pt⁰ ratios from XPS characterization for fresh and used catalysts. Fresh catalyst additionally reduced.

Sample	Pt ²⁺ /Pt ⁰ ratio
Fresh catalyst additionally reduced	0.6
After cycle 1	0.7
After cycle 3	0.6
After cycle 5	0.6

morphological changes and changes in metallic phase dispersion.

Deconvoluted Pt 4f XPS spectra of fresh catalyst and catalysts used in several reaction cycles are shown in Fig. 13, where peaks located at binding energy values around 71 and 75 eV are ascribed to metallic platinum, while those around 73 and 76 eV correspond to Pt²⁺ for the two spin-orbit splits (Pt 4f_{7/2} and Pt 4f_{5/2}) [68]. Binding energy values and Pt²⁺/Pt⁰ ratios calculated from the intensity of the peaks for fresh and used catalyst are summarized in Table 5. It has been reported in literature [69–71] that changes in Pt nanoparticle size can induce changes in binding energy and Pt²⁺/Pt⁰ ratio and, in turn, higher charged metal nanoparticles induce higher catalytic activity. However, in this work no significant trend and changes in binding energies can be observed, indicating that charge transfer properties are not modified significantly along the cycles and may not be related to changes in hydrogen production. Likewise, changes observed in Pt²⁺/Pt⁰ ratio may be related to the redispersion of the metal phase that can be observed in Fig. 11, particularly after cycle 1 and most probably due to Ostwald ripening, result in a higher prevalence of low coordination sites such as corners and edges.

To deepen on the influence of Pt dispersion on the catalytic performance, a five-cycle reuse test was carried out using a fresh catalyst that was reduced for an additional hour previous to use. In this case, the fresh catalyst showed a nanoparticle size distribution displaced to smaller values (Fig. 15) and slightly higher Pt²⁺/Pt⁰ ratio (Table 6). Minor changes in nanoparticle size distribution were observed after cycle 1, but

again, an increase in Pt²⁺/Pt⁰ was observed after cycle one. This catalyst showed slightly higher production of hydrogen during the first two cycles, however no significant quantitative differences were observed between the two catalysts after three cycles (Fig. 14). Therefore, catalysts with higher prevalence of small nanoparticles produce more hydrogen, but this nanoparticle size range is unstable under APR reaction conditions. However, the catalysts tested show minor differences in nanoparticle size distribution and the relationship between catalytic performance and metal nanoparticle reduction degree and structure cannot be unequivocally assessed.

4. Conclusions

The APR of compounds representative of biooil aqueous fraction has been investigated with the aim to produce bio-hydrogen and/or bio-alkanes as valorisation route for this wastewater biorefinery stream. The processability of model has been evaluated through substrate conversion, carbon-to-gas yield and production of hydrogen and alkanes, showing similar and even better values than those reported for common substrates used in APR such as sugars, polyols, etc. Maximum values of organic matter conversion were obtained for levoglucosan and furfural (90–95%), being hydroxyacetone and acetic acid the more refractory (c. a 70%) in this sense. Good matching was found between conversion and carbon-to-gas yield, indicating that most of the organic matter converted follow a route to hydrogen and/or alkanes, instead of undesirable water-soluble byproducts. Accordingly, high hydrogen yields values, as high as 50 mmol/gTOC was obtained for hydroxyacetone, while acetic acid was mainly converted to methane (30 mmol/gTOC). The catalyst used showed a high stability, with nearly constant catalytic activity after 20 h of operation in five consecutive batches, which is essential for process feasibility. The results suggest that AFB fraction constitutes a promising option for bio-hydrogen production by APR.

CRediT authorship contribution statement

Jéssica Justicia: Investigation, Data curation, Formal analysis, Writing – original draft, Review & Editing. **José Alberto Baeza:** Validation, Writing – original draft. **Adriana S. de Oliveira:** Validation, Writing – original draft. **Luisa Calvo:** Conceptualization, Funding acquisition. **Francisco Heras:** Conceptualization, Formal analysis, Supervision, Writing – review & editing. **Miguel A. Gilarranz:** Supervision, Writing – review & editing, Funding acquisition.

Declaration of competing interest

The authors declare the following financial interests/personal relationships which may be considered as potential competing interests: Francisco Heras reports financial support was provided by Autonomous University of Madrid and Project BIOTRES-CM (S2018/EMT-4344),

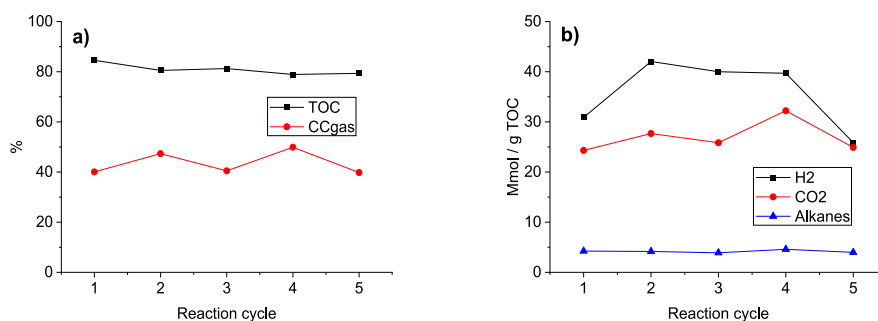


Fig. 14. Stability of additionally reduced Pt/CB catalyst in five consecutive reaction cycles a) TOC conversion and CC gas, b) Gas production (1% levoglucosan, 220 °C, 4 h).

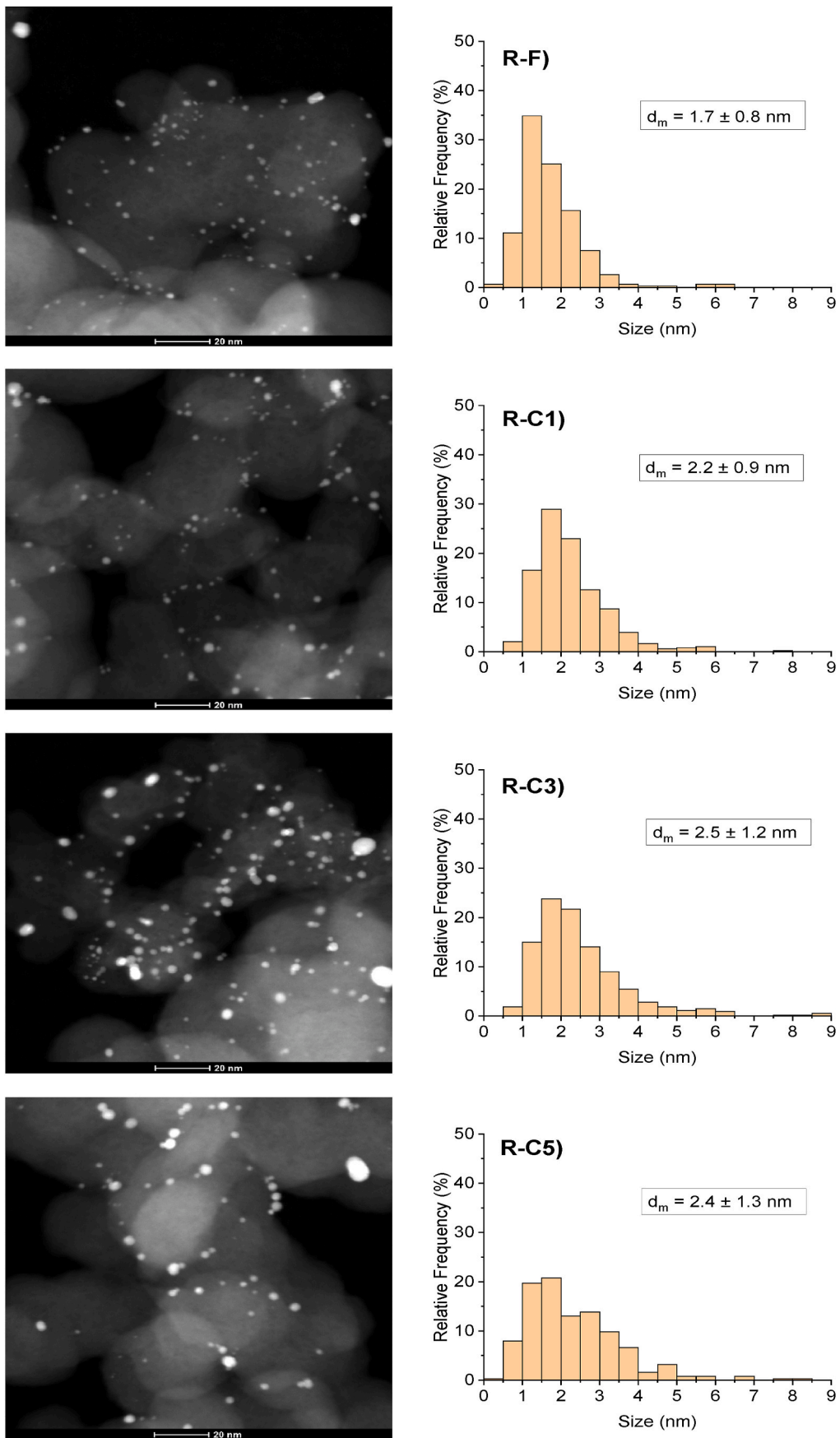


Fig. 15. STEM images of additionally reduced catalyst: F) fresh, C1) cycle 1, C3) cycle 3 and C5) cycle 5.

funded by the Community of Madrid and the European Regional Development Fund. Francisco Heras reports a relationship with Autonomous University of Madrid that includes: employment.

Acknowledgements

The authors thank financial support from Community of Madrid thought research network BIO3 (P2018/EMT- 4344).

References

- [1] T. Imam, S. Capareda, Characterization of bio-oil, syn-gas and bio-char from switchgrass pyrolysis at various temperatures, *J. Anal. Appl. Pyrolysis* 93 (2012) 170–177.
- [2] C. Mukarakate, R.J. Evans, S. Deutch, T. Evans, A.K. Starace, J. Dam, M.J. Watson, K. Magrini, Reforming biomass derived pyrolysis bio-oil aqueous phase to fuels, *Energy Fuels* 31 (2017) 1600–1607.
- [3] R. Rauch, J. Hrbek, Hofbauer, Biomass gasification for synthesis gas production and applications of the syngas, *WIREs Energy Environ.* 3 (2014) 343–362.
- [4] O.M. Larina, V.A. Sinelshchikov, G.A. Sytchev, Comparison of thermal conversion methods of different biomass types into gaseous fuel, *J. Phys. Conf. Ser.* 774 (2016), 012137.
- [5] O.A. Fakayode, E.A.A. Aboagarib, Co-pyrolysis of lignocellulosic and macroalgae biomasses for the production of biochar – a review, *Bioresour. Technol.* 297 (2020), 122408.
- [6] C. Pan, A. Chen, Z. Liu, P. Chen, H. Lou, X. Zheng, Aqueous-phase reforming of the low-boiling fraction of rice husk pyrolyzed bio-oil in the presence of platinum catalyst for hydrogen production, *Bioresour. Technol.* 125 (2012) 335–339.
- [7] W. Li, C. Pan, L. Sheng, Z. Liu, P. Chen, H. Lou, X. Zheng, Upgrading of high-boiling fraction of bio-oil in supercritical methanol, *Bioresour. Technol.* 102 (2011) 9223–9228.
- [8] M.B. Shemfe, S. Gu, P. Ranganathan, Techno-economic performance analysis of biofuel production and miniature electric power generation from biomass fast pyrolysis and bio-oil upgrading, *Fuel* 143 (2015) 361–372.
- [9] J. Remon, F. Broust, J. Valette, Y. Chhiti, I. Alava, A.R. Fernandez-Akarregi, J. Arauzo, L. Garcia, Production of a hydrogen-rich gas from fast pyrolysis bio-oils: comparison between homogeneous and catalytic steam reforming routes, *Int. J. Hydrogen Energy* 39 (2014) 171–182.
- [10] B.A. Black, W.E. Michener, K.J. Ramirez, M.J. Bidy, B.C. Knott, M.W. Jarvis, J. Olstad, O.D. Mante, D.C. Dayton, G.T. Beckham, Aqueous stream characterization from biomass fast pyrolysis and catalytic fast pyrolysis, *ACS Sustain. Chem. Eng.* 4 (2016) 6815–6827.
- [11] T.P. Vispute, G.W. Huber, Production of hydrogen, alkanes and polyols by aqueous phase processing of wood-derived pyrolysis oils, *Green Chem.* 11 (2009) 1433–1445.
- [12] B. Valle, A. Remiro, A.T. Aguayo, J. Bilbao, A. Gayubo, Catalysts of Ni/ α -Al₂O₃ and Ni/La₂O₃- α -Al₂O₃ for hydrogen production by steam reforming of bio-oil aqueous fraction with pyrolytic lignin retention, *Int. J. Hydrogen Energy* 38 (2013) 1307–1318.
- [13] V.N. Kalekar, P.D. Vaidya, Hydrogen production by reforming of sodium alginate in the liquid phase over Pt/C catalyst, *Ind. Eng. Chem. Res.* 60 (2021) 9755–9763.
- [14] M. Khodabandehloo, A. Larimi, F. Khorasheh, Comparative process modeling and techno-economic evaluation of renewable hydrogen production by glycerol reforming in aqueous and gaseous phases, *Energy Convers. Manag.* 225 (2020), 113483.
- [15] M. Martin, I.E. Grossmann, Optimal simultaneous production of hydrogen and liquid fuels from glycerol: integrating the use of biodiesel byproducts, *Ind. Eng. Chem. Res.* 53 (2014) 7730–7745.
- [16] I. Coronado, M. Stekrova, M. Reinikainen, P. Simell, L. Lefferts, J. Lehtonen, A review of catalytic aqueous-phase reforming of oxygenated hydrocarbons derived from biorefinery water fractions, *Int. J. Hydrogen Energy* 41 (2016) 11003–11032.
- [17] R.D. Cortright, R.R. Davda, J.A. Dumesic, Hydrogen from catalytic reforming of biomass-derived hydrocarbons in liquid water, *Nature* 418 (2002) 964–967.
- [18] R.R. Davda, J.W. Shabaker, G.W. Huber, R.D. Cortright, J.A. Dumesic, A review of catalytic issues and process conditions for renewable hydrogen and alkanes by aqueous-phase reforming of oxygenated hydrocarbons over supported metal catalysts, *Appl. Catal., B* 56 (2005) 171–186.
- [19] T. Xie, B.J. Hare, P.J. Meza-Morales, C. Sievers, R.B. Getman, Identification of the active sites in the dehydrogenation of methanol on Pt/Al₂O₃ catalysts, *J. Phys. Chem. C* 124 (2020) 19015–19023.
- [20] H. Harju, G. Pipitone, L. Lefferts, Influence of the catalyst particle size on the aqueous phase reforming of n-butanol over Rh/ZrO₂, *Front. Chem.* 8 (2020) 17.
- [21] R.R. Davda, J.W. Shabaker, G.W. Huber, R.D. Cortright, J.A. Dumesic, Aqueous-phase reforming of ethylene glycol on silica-supported metal catalysts, *Appl. Catal., B* 43 (2003) 13–26.
- [22] A. Fasolini, E. Lombardi, T. Tabanelli, F. Basile, Microemulsion derived titania nanospheres: an improved Pt supported catalyst for glycerol aqueous phase reforming, *Nanomaterials* 11 (2021) 1175.
- [23] M. Alvear, A. Aho, I.L. Simakova, H. Grénman, T. Salmi, D.Y. Murzin, Aqueous phase reforming of alcohols over a bimetallic Pt-Pd catalyst in the presence of formic acid, *Chem. Eng. J.* 398 (2020), 125541.
- [24] P. Gogoi, N. Kanna, P. Begum, R.C. Deka, C.V.V. Satyanarayana, T. Raja, Controlling and stabilization of Ru nanoparticles by tuning the nitrogen content of the support for enhanced H₂ production through aqueous-phase reforming of glycerol, *ACS Catal.* 10 (2020) 2489–2507.
- [25] Xing, R., Dgle, V.L., Flake, M., Kovarik, L., Albrecht, K.O., Deshmane, C., Dagle, R. A. Steam reforming of fast pyrolysis-derived aqueous phase oxygenates over Co, Ni, and Rh metals supported on MgAl₂O₄, *Catal. Today* 269, 166–174.
- [26] M. El Doukkali, A. Iriondo, J.F. Cambra, L. Jalowiecki-Duhamel, A.S. Mamede, F. Dumeignil, P.L. Arias, Pt monometallic and bimetallic catalysts prepared by acid sol–gel method for liquid phase reforming of bioglycerol, *J. Mol. Catal. Chem.* 368–369 (2020) 125–136.
- [27] S. Irmak, I. Öztürk, Hydrogen rich gas production by thermocatalytic decomposition of kenaf biomass, *Int. J. Hydrogen Energy* 35 (2010) 5312–5317.
- [28] A. Seretis, P. Tsiakaras, Aqueous phase reforming (APR) of glycerol over platinum supported on Al₂O₃ catalyst, *Renew. Energy* 85 (2016) 1116–1126.
- [29] G. Pipitone, G. Zoppi, R. Pirone, S. Bensaid, A critical review on catalyst design for aqueous phase reforming, *Int. J. Hydrogen Energy* 47 (2022) 151–180.
- [30] T. Kim, H. Kim, K. Jeong, H. Chae, S. Jeong, C. Lee, C. Kim, Catalytic production of hydrogen through aqueous-phase reforming over platinum/ordered mesoporous carbon catalysts, *Green Chem.* 13 (2011) 1718–1728.
- [31] M.M. Rahman, Aqueous-phase reforming of glycerol over carbon-nanotube-supported catalysts, *Catal. Lett.* 150 (2020) 2674–2687.
- [32] A.K.K. Vikla, I. Simakova, Y. Demidova, E.G. Keim, L. Calvo, M.A. Gilarranz, Songbo He, K. Seshan, Tuning Pt characteristics on Pt/C catalyst for aqueous-phase reforming of biomass-derived oxygenates to bio-H₂, *Appl Catal., A* 610 (2021), 117963.
- [33] A.V. Kirilin, A.V. Tokarev, L.M. Kustov, T. Salmi, J.-P. Mikkola, D.Y. Murzin, Aqueous phase reforming of xylitol and sorbitol: comparison and influence of substrate structure, *Appl Catal., A* 435–436 (2012) 172–180.
- [34] J.W. Shabaker, G.W. Huber, J.A. Dumesic, Aqueous-phase reforming of oxygenated hydrocarbons over Sn-modified Ni catalysts, *J. Catal.* 222 (2004) 180–191.
- [35] P. Lozano, A.I. Simon, L. Garcia, J. Ruiz, M. Oliva, J. Arauzo, Influence of the Ni-Co/Al-Mg catalyst loading in the continuous aqueous phase reforming of the bio-oil aqueous fraction, *Processes* 9 (2021) 81.
- [36] K. Koichumanova, A.K.K. Vikla, R. Cortese, F. Ferrante, K. Seshan, D. Duca, L. Lefferts, In situ ATR-IR studies in aqueous phase reforming of hydroxyacetone on Pt/ZrO₂ and Pt/AlO(OH) catalysts: the role of aldol condensation, *Appl. Catal., B* 232 (2018) 454–463.
- [37] A. Arandia, I. Coronado, A. Remiro, A.G. Gayubo, M. Reinikainen, Aqueous-phase reforming of bio-oil aqueous fraction over nickel-based catalysts, *Int. J. Hydrogen Energy* 44 (2019) 13157–13168.
- [38] T. Nozawa, Y. Mizukoshi, A. Yoshida, S. Naito, Aqueous phase reforming of ethanol and acetic acid over TiO₂ supported Ru catalysts, *Appl. Catal., B* 146 (2014) 221–226.
- [39] Y. Wei, H. Lei, Y. Liu, L. Wang, L. Zhu, X. Zhang, G. Yadavalli, B. Ahring, S. Chen, Renewable hydrogen produced from different renewable feedstock by aqueous-phase reforming process, *J. Sustain. Bioenergy Syst.* 4 (2014) 113–127.
- [40] J. Lemus, J. Bedia, L. Calvo, I.L. Simakova, D.Y. Murzin, B.J.M. Etzold, J. Rodriguez, M.A. Gilarranz, Improved synthesis and hydrothermal stability of Pt/C catalysts based on size-controlled nanoparticles, *Catal. Sci. Technol.* 6 (2016) 5196–5206.
- [41] A.S. Oliveira, T. Cordero-Lanzac, J.A. Baeza, L. Calvo, F. Heras, J.J. Rodriguez, M. A. Gilarranz, Continuous aqueous phase reforming of a synthetic brewery wastewater with Pt/C and PtRe/C catalysts for biohydrogen production, *Chemosphere* 281 (2021), 130885.
- [42] N. Alonso, M.A. Gilarranz, F. Heras, J.J. Rodriguez, S. Eser, Effects of heat treatment on the structure of LDPE-derived solid carbons, *Chem. Eng. J.* 172 (2–3) (2011) 1126–1136.
- [43] A. Angeles-Pascual, Structural atomic study in platinum heterogeneous catalyst by aberration-corrected STEM, *Appl. Surf. Sci.* 566 (2021), 150745.
- [44] T. Zhan, S. Wu, H. Ma, C. Yue, Z. Huang, W. Liu, J. Teng, D. Li, S. Wang, H. Tan, Production of biofuel intermediates from furfural via aldol condensation over K₂O clusters containing N-doped porous carbon materials with shape selectivity, *Microporous Mesoporous Mater.* 281 (2019) 101–109.
- [45] H. Simsir, N. Eltugral, S. Karagoz, Hydrothermal carbonization for the preparation of hydrochars from glucose, cellulose, chitin, chitosan and wood chips via low-temperature and their characterization, *Bioresour. Technol.* 246 (2017) 82–87.
- [46] A. Chen, P. Chen, D. Cao, H. Lou, Aqueous-phase reforming of the low-boiling fraction of bio-oil for hydrogen production: the size effect of Pt/Al₂O₃, *Int. J. Hydrogen Energy* 40 (2015) 14798–14805.
- [47] Y. Shao, X. Hu, Z. Zhang, K. Sun, G. Gao, T. Wei, S. Zhang, S. Hu, J. Xiang, Y. Wang, Direct conversion of furfural to levulinic acid/ester in dimethylmethane: understanding the mechanism for polymerization, *Green Energy Environ.* 4 (2019) 400–413.
- [48] N. Luo, X. Fu, F. Cao, T. Xiao, P.P. Edwards, Glycerol aqueous phase reforming for hydrogen generation over Pt catalyst – effect of catalyst composition and reaction conditions, *Fuel* 87 (2008) 3483–3489.
- [49] Y. Wang, D. Zhao, D. Rodriguez-Padron, C. Len, Recent advances in catalytic hydrogenation of furfural, *Catalysts* 9 (2019) 796.
- [50] D.A. Sladkovskiy, L.I. Godina, K.V. Semikin, E.V. Sladkovskaya, D.A. Smirnova, D. Y. Murzin, Process design and techno-economic analysis of hydrogen production by aqueous phase reforming of sorbitol, *Chem. Eng. Res. Des.* 134 (2018) 104–116.
- [51] N.D. Subramanian, J. Callison, C.R.A. Catlow, P.P. Wells, N. Dimitratos, Optimised hydrogen production by aqueous phase reforming of glycerol on Pt/Al₂O₃, *Int. J. Hydrogen Energy* 41 (2016) 18441–18450.

- [52] A. Aho, C. Rosales, K. Eränen, T. Salmi, D.Y. Murzin, H. Grenman, Biohydrogen from dilute side streams - influence of reaction conditions on the conversion and selectivity in aqueous phase reforming of xylitol, *Biomass Bioenergy* 138 (2020), 105590.
- [53] G. Pipitone, G. Zoppi, S. Bocchini, A.M. Rizzo, D. Chiaramontic, R. Pirone, S. Bensaid, Aqueous phase reforming of the residual waters derived from lignin-rich hydrothermal liquefaction: investigation of representative organic compounds and actual biorefinery streams, *Catal. Today* 345 (2020) 237–250.
- [54] G. Pipitone, G. Zoppi, S. Ansaloni, S. Bocchini, F.A. Deorsola, R. Pirone, S. Bensaid, Towards the sustainable hydrogen production by catalytic conversion of C-laden biorefinery aqueous streams, *Chem. Eng. J.* 377 (2019), 120677.
- [55] J. Callison, N.D. Subramanian, S.M. Rogers, A. Chutia, D. Gianolio, C.R.A. Catlow, P.P. Wells, N. Dimitratos, Directed aqueous-phase reforming of glycerol through tailored platinum nanoparticles, *Appl. Catal., B* 238 (2018) 618–628.
- [56] M.M. Rahman, H₂ production from aqueous-phase reforming of glycerol over Cu-Ni bimetallic catalysts supported on carbon nanotubes, *Int. J. Hydrogen Energy* 40 (2015) 14833–14844.
- [57] P.J. Dietrich, R.J. Lobo-Lapidus, T. Wu, A. Sumer, M.C. Akatay, B.R. Fingland, N. Guo, J.A. Dumesic, C.L. Marshall, E. Stach, J. Jellinek, W.N. Delgass, F. H. Ribeiro, J.T. Miller, Aqueous phase glycerol reforming by PtMo bimetallic nanoparticle catalyst: product selectivity and structural characterization, *Top. Catal.* 55 (2012) 53–69.
- [58] L. Zhang, A.M. Karim, M.H. Engelhard, Z. Wei, D.L. King, Y. Wang, Correlation of Pt–Re surface properties with reaction pathways for the aqueous-phase reforming of glycerol, *J. Catal.* 287 (2012) 37–43.
- [59] D. King, Y. Wang, L. Zhang, A. Karim, D. Heldebrant, Biomass-derived Liquids Distributed (Aqueous Phase) Reforming, DOE Hydrogen and fuel cells program review, 2011. May 10, 2011).
- [60] A.S. Oliveira, J.A. Baeza, L. Calvo, N. Alonso-Morales, F. Heras, J.J. Rodriguez, M. A. Gilarranz, Production of hydrogen from brewery wastewater by aqueous phase reforming with Pt/C catalysts, *Appl. Catal., B* 245 (2019) 367–375.
- [61] S. Helle, N.M. Bennett, K. Lau, J.H. Matsui, S.J.B. Duff, A kinetic model for production of glucose by hydrolysis of levoglucosan and cellobiosan from pyrolysis oil, *Carbohydr. Res.* 342 (2007) 2365–2370.
- [62] A.B. Bindwal, P.D. Vaidya, Kinetics of aqueous-phase hydrogenation of levoglucosan over Ru/C catalyst, *Ind. Eng. Chem. Res.* 52 (2013) 17781–17789.
- [63] S. Irmak, B. Meryemoglu, B.K. Ozsel, A. Hasanoglu, O. Erbatur, Improving activity of Pt supported metal catalysts by changing reduction method of Pt precursor for hydrogen production from biomass, *Int. J. Hydrogen Energy* 40 (2015) 14826–14832.
- [64] B. Saenz de Miera, A.S. Oliveira, J.A. Baeza, L. Calvo, J.J. Rodriguez, M. A. Gilarranz, Treatment and valorisation of fruit juice wastewater by aqueous phase reforming: effect of pH, organic load and salinity, *J. Clean. Prod.* 252 (2020), 119849.
- [65] B. Kaya, S. Irmak, A. Hasanoglu, O. Erbatur, Developing Pt based bimetallic and trimetallic carbon supported catalysts for aqueous-phase reforming of biomass-derived compounds, *Int. J. Hydrogen Energy* 40 (2015) 3849–3858.
- [66] G. Pipitone, D. Tosches, S. Bensaid, A. Galia, R. Pirone, Valorization of alginate for the production of hydrogen via catalytic aqueous phase reforming, *Catal. Today* 304 (2018) 153–164.
- [67] S. Neumann, J. Schröder, F. Bizzoto, M. Arenz, A. Dworzak, M. Oezaslan, M. Bäumer, S. Kunz, Halide-induced leaching of Pt nanoparticles – manipulation of particle size by controlled Ostwald ripening, *Chem. Nano Mat.* 5 (2019) 462–471.
- [68] M.A. Álvarez-Montero, L.M. Gómez-Sainero, A. Mayoral, I. Diaz, R.T. Baker, J. J. Rodriguez, Hydrodechlorination of chloromethanes with a highly stable Pt on activated carbon catalyst, *J. Catal.* 279 (2011) 389–396.
- [69] S.A. Gurevich, D.S. Il'yushchenkov, D.A. Yavsin, N.V. Glebova, A.A. Nechitailov, N. K. Zelenina, A.A. Tomasov, Charge state and activity of Pt/C catalysts in oxygen reduction reaction, *Russ. J. Electrochem.* 53 (6) (2017) 567–574.
- [70] Q.Q. Yan, D.X. Wu, S.Q. Chu, Z.Q. Chen, Y. Lin, M.X. Chen, J. Zhang, X.J. Wu, H. W. Liang, Reversing the charge transfer between platinum and sulfur-doped carbon support for electrocatalytic hydrogen evolution, *Nat. Commun.* 10 (2019) 4977.
- [71] A. Elangovan, J. Xu, A. Sekar, S. Rajendran, B. Liu, J. Li, Platinum deposited nitrogen-doped vertically aligned carbon nanofibers as methanol tolerant catalyst for oxygen reduction reaction with improved durability, *Appl. Nanosci.* 2 (2021) 303–331.